The Affinities for the Two Substrate Water Binding Sites in the O_2 Evolving Complex of Photosystem II Vary Independently during S-State Turnover

Warwick Hillier‡ and Tom Wydrzynski*

Research School of Biological Sciences, The Australian National University, Canberra, ACT 0200, Australia

Received October 5, 1999; Revised Manuscript Received December 6, 1999

ABSTRACT: The first determinations of substrate water binding to the O_2 evolving complex in photosystem II as a complete function of the S states have been made. $H_2{}^{18}O$ was rapidly injected into spinach thylakoid samples preset in either the S_0, S_1, S_2, or S_3 states, and the rate of ^{18}O incorporation into the O_2 produced was determined by time-resolved mass spectrometry. For measurements at $m/e = 34$ (i.e., for the $^{16}O^{18}O$ product), the rate of ^{18}O incorporation in all S states shows biphasic kinetics, reflecting the binding of the two substrate water molecules to the catalytic site. The slow phase kinetics yield rate constants at 10 °C of 8 ± 2, 0.021 ± 0.002, 2.2 ± 0.3, and 1.9 ± 0.2 s^{-1} for the S_0, S_1, S_2, and S_3 states, respectively, while the fast phase kinetics yield a rate constant of 36.8 ± 1.9 s^{-1} for the S_3 state but remain unresolvable (>100 s^{-1}) for the S_0, S_1, and S_2 states. Comparisons of the ^{18}O exchange rates reveal that the binding affinity for one of the substrate water molecules first increases during the S_0 to S_1 transition, then decreases during the S_1 to S_2 transition, but stays the same during the S_2 to S_3 transition, while the binding affinity for the second substrate water molecule undergoes at least a 5-fold increase on the S_2 to S_3 transition. These findings are discussed in terms of two independent Mn^{III} substrate binding sites within the O_2 evolving complex which are separate from the component that accumulates the oxidizing equivalents. One of the Mn^{III} sites may only first bind a substrate water molecule during the S_2 to S_3 transition.

Even though considerable spectroscopic and biochemical information is available on the oxygen evolving complex (OEC)[1] in photosytem II (PSII) of green plants, the mechanism by which water is photochemically oxidized to molecular oxygen still remains a matter of intense debate and speculation. A significant problem has been the difficulty in obtaining a highly resolved molecular structure of the OEC (*1*), although it is well-established that the OEC contains a redox-active cluster of four Mn ions. The Mn ions are believed to be ligated, at least in part, to amino acid residues of the reaction center polypeptide D1 (*2*, *3*).

The observation that has had the greatest impact on our understanding of the O_2 evolving mechanism came from the early work of Joliot in which he showed that the O_2 produced by a series of single-turnover light flashes follows a basic periodicity of 4 (*4*). The kinetic framework to explain this phenomenon was developed by Kok and co-workers and indicated that the OEC cycles through five intermediary states (S_0, S_1, S_2, S_3, S_4) during sequential photoactivations of PSII (*5*). Upon reaching the S_4 state, O_2 is immediately released, and the cycle begins again. Several detailed chemical models depicting the S states have since been proposed, based largely on spectroscopic studies of the functional Mn and its surroundings (*6*−*12*). Of central importance to all of the models is the role that a redox-active tyrosine (Y_Z) may have in the reaction mechanism (*13*, *14*).

To help ascertain the various proposals for the O_2 evolving mechanism, it would be of considerable advantage to have a direct means to measure the binding of the substrate water to the catalytic site. Unfortunately, this is difficult to achieve experimentally since the substrate water cannot be readily distinguished from the solvent water, unless another noninteracting solvent can be found to lower the water content (activity) of the sample (*15*). On the other hand, substrate interactions at the catalytic site can be monitored by using mass spectrometric techniques. In this case, the amount of oxygen isotope incorporated into the O_2 produced is measured after isotopically defined water is added to the sample (*16*−*18*). In the early studies using this approach, it was found that water binds to the OEC at least during the last step of the reaction sequence (i.e., during the S_3 to S_4 to S_0 transition), though the kinetic resolution at the time was not sufficient enough to determine the precise rates of isotopic exchange.

Recently, we have been able to improve the time resolution for the mass spectrometric measurements (*19*) and from a detailed analysis of the data obtained at $m/e = 34$ showed that there are two separate ^{18}O exchange processes in the S_3 state of the OEC, reflecting the individual binding affinities for the two substrate water molecules (20). Upon repeating these measurements on PSII-containing samples in the S_2 state, a similar biphasicity in the ^{18}O exchange kinetics was also observed (*21*). In the present communication, we complete the series of measurements as a function of the S

* Correspondence should be addressed to this author at the Research School of Biological Sciences, The Australian National University, Canberra, ACT 0200, Australia. Tel: +61 (02) 6249 5892. Fax: +61 (02) 6279 8056. Email: TOM@rsbs.anu.edu.au.

‡ Current address: Department of Chemistry, Michigan State University, East Lansing, MI 48825.

[1] Abbreviations: PSII, photosystem II; OEC, O_2 evolving complex; S_n state (for $n = 0, 1, 2, 3, 4$), intermediate redox states of the O_2 evolving complex.

10.1021/bi992318d CCC: $19.00
Published on Web 03/22/2000

states and report the ^{18}O exchange kinetics for PSII-containing samples in the S_0 and S_1 states. In these S states as well, there remains a distinct biphasic behavior in the ^{18}O exchange measured at $m/e = 34$. From the complete analysis of the S-state dependence in ^{18}O exchange, it becomes clear for the first time that one substrate water molecule is bound to the OEC in PSII throughout the entire S-state cycle, though its binding affinity varies with S-state turnover, while the second substrate water molecule binds to the OEC *separately* in at least the S_3 state. The implications of these results are discussed in terms of the organization of the catalytic site.

MATERIALS AND METHODS

Thylakoid samples were prepared from hydroponically grown spinach by grinding the leaves in a medium containing 30 mM Mes buffer (pH 6.5), 350 mM sorbitol, 15 mM NaCl, and 5 mM $MgCl_2$, in a Waring blender for 10 s. The homogenate was filtered through two layers of cotton gauze and two layers of nylon cloth (20 μm mesh size) and centrifuged for 5 min at 5000 rpm in a Sorval GSA rotor. The thylakoid pellet was then resuspended and washed once in a medium containing 30 mM Hepes buffer (pH 6.8), 400 mM sucrose, 15 mM NaCl, and 5 mM $MgCl_2$, before being frozen as small beads in liquid N_2 and stored at -80 °C. Typical rates of O_2 evolution for these samples were ~ 240 μM O_2 (mg of Chl)$^{-1}$ h^{-1} using 400 μM *p*-phenylbenzoquinone and 500 μM $K_3Fe(CN)_6$ as the added electron acceptors.

Mass spectrometric measurements of the flash-induced O_2 produced by the thylakoid samples were made at $m/e = 34$ and $m/e = 36$ (i.e., for the mixed labeled $^{16}O^{18}O$ and double labeled $^{18}O^{18}O$ products, respectively) with an in-line mass spectrometer (Vacuum Generation MM6, Winford, U.K.). A specially designed sample chamber as described earlier (*19*), but having a smaller internal volume (160 μL) (*20*), was used for the rapid injection of 25 μL of $H_2{}^{18}O$ (98.5% enrichment, ISOTECH, Miamisberg, OH) into the sample. The final ^{18}O enrichment after injection was 12.0 ± 0.5%. Samples were variously activated with saturating light flashes (fwhh ~ 8 μs) from three separate xenon flash lamps (FX-193 lamp, 4 μF at 1 kV capacitor, EG & G, Salem, MA) optically coupled to the sample chamber via a 3-to-1 fiber optic. The various injection/flash protocols (see below) were controlled by a computer, and accurate timing intervals were established using a digital oscilloscope. Measurements were made in the absence of an electron acceptor at a sample concentration of 0.5 mg of Chl mL^{-1} at 10 °C for optimal S/N. Under low-temperature conditions, the deactivation reactions of the S_2 and S_3 states in spinach thylakoids are considerably slowed (*22*), and thus there is no undue scrambling of the S states during the flash sequences. The oscillatory pattern in the mass measurements gives a miss parameter of about 16% and a double hit parameter of about 3.5% when analyzed according to the Kok model (*19*).

The ^{18}O exchange kinetics were determined for the different S states using the injection/flash protocols depicted in Figure 1. Prior to loading, the samples were thawed in the dark at room temperature and given one saturating preflash followed by a 10 min dark period in order to enrich the S_1-state population. The S_1-enriched samples were then loaded into the sample chamber in the dark, equilibrated to 10 °C for 10−12 min, and then given a number of *activating*

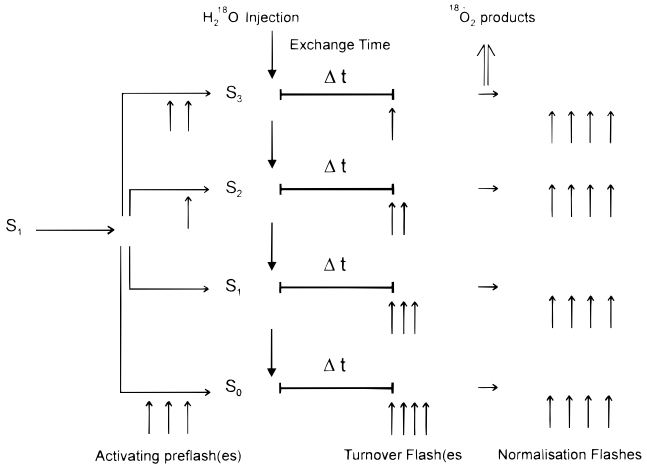

FIGURE 1: Injection/flash protocols for measuring the ^{18}O exchange in the various S states. S_1-enriched, spinach thylakoid samples were subjected to a series of *activating* flashes at 10 °C to generate a particular S state. $H_2{}^{18}O$ was then rapidly injected ($t_{1/2} \sim 4$ ms) and a variable delay time (Δt) given before a series of *turnover* flashes were provided to generate the photoproduced, ^{18}O-labeled dioxygen which was measured either at $m/e = 34$ or at $m/e = 36$. Subsequently, a series of four *normalization* flashes were given to the sample for standardization purposes. See text for details.

flashes (spaced 1 s apart) according to the protocols in Figure 1. At a given S state, $H_2{}^{18}O$ was rapidly injected into the chamber [$t_{1/2(\text{mixing})} \sim 4$ ms], and a variable delay time (4 ms $> \Delta t <$ 200 s) was provided to allow the water bound in the OEC to exchange with the added $H_2{}^{18}O$. After the delay time, a number of rapid *turnover* flashes (spaced 10 ms apart) were then applied to advance the sample through to the S_3 to S_4 to S_0 transition being measured whereupon the mass ratio of the photogenerated O_2 (Y_M) was determined. Following this, a number of *normalization* flashes (spaced 20 s apart) were given and their separate O_2 yields [$Y_{n(1\rightarrow4)}$] measured. The O_2 signals were recorded on an x−t plotter and the amplitudes analyzed as described earlier (*19*).

To properly evaluate the ^{18}O exchange kinetics, the O_2 produced during a particular S_3 to S_4 to S_0 transition had to be adjusted for background O_2 signals. The background O_2 due to the injection (Y_{inj}) was corrected as described earlier (*20*). The O_2 contributions due to double hits after $H_2{}^{18}O$ injection during the multiple *turnover* flashes (Y_{x2}) were determined at each delay time, Δt, used in a particular *turnover* flash sequence less 1 flash and subtracted from Y_M. Of course, for the S_3-state measurements only one *turnover* flash is given, and so in this case there is no need to correct for a double hit contribution. The dependence of double hits on Δt in the various *turnover* flash sequences is given in Figures 3−5 in the Ph.D thesis by W. Hillier (*23*). Finally, to correct for variations between measurements due to differences in membrane permeability, sample concentrations, and S-state deactivation, Y_M was normalized to the sum of the four flashes following the *turnover* sequence. Thus, the O_2 yield values used to determine the ^{18}O exchange kinetics were adjusted as follows:

$$Y_N = (Y_M - Y_{\text{inj}} - Y_{x2})/\Sigma Y_{n(1\rightarrow4)} \quad (1)$$

For comparative purposes, the Y_N value at each delay time, Δt, was divided by the Y_N value determined at the longest delay time at which isotopic exchange was complete.

The data at very short delay times had to be further corrected to compensate for the increasing levels of ^{18}O enrichment and decreasing levels of sample concentration during the injection response ($k_{inj} = 175\ s^{-1}$) (*20*). Thus, for the Y_N values at $\Delta t < 10$ ms, the following adjustment was applied (*20, 23*):

$$Y_{C(t)} = Y_{N(t)} \frac{1}{[1 - \exp(-175t)][(1 + \Delta\text{chl})(\exp -175t)]} \quad (2)$$

where

$$\Delta\text{chl} = \frac{\{[\text{chl}]_{(t=0)} - [\text{chl}]_{(t=\infty)}\}}{[\text{chl}]_{(t=\infty)}}$$

for Y_N values at $\Delta t > 10$ ms, $Y_C = Y_N$.

The plots of Y_C vs Δt at $m/e = 36$ exhibit only a single kinetic phase and were analyzed with a simple exponential function (*19, 20*), i.e.:

$$^{36}Y_C = [1 - \exp(-^{36}kt)] \quad (3)$$

On the other hand, the plots of Y_C vs Δt at $m/e = 34$ are clearly biphasic and were analyzed as the sum of two exponential functions (*20*), i.e.:

$$^{34}Y_C = 0.57[1 - \exp(-^{34}k_2t)] + 0.43[1 - \exp(-^{34}k_1t)] \quad (4)$$

Sigma Plot was used to fit the data to eqs 3 and 4.

RESULTS

The complete S-state dependence in the ^{18}O exchange at 10 °C for spinach thylakoid samples is shown in Figure 2. The corrected/normalized yields of O_2 (Y_C) measured at $m/e = 34$ for the mixed labeled $^{16}O^{18}O$ product (left side of the figure) and at $m/e = 36$ for the double labeled $^{18}O^{18}O$ product (right side of the figure) are plotted as a function of the delay time, Δt, between the injection of $H_2{}^{18}O$ into the sample and the *turnover* flash sequences used to monitor the various S states, as described by the injection/flash protocols given in Figure 1. The insets in the panels on the left side of the figure show an expanded time ordinate to reveal the fast kinetics in the $m/e = 34$ data. The solid lines represent the best fits to the data points based on eqs 3 and 4 for the $m/e = 36$ and $m/e = 34$ data, respectively. The exchange rates from the corresponding kinetic fits are given in Table 1. The results for the S_3 and S_2 states have been reported earlier (*20, 21*).

There are several striking features in the data shown in Figure 1. For all S states, the ^{18}O exchange measured at $m/e = 34$ reveals biphasic behavior with a kinetically resolvable slow phase. The biphasic behavior in the S_3 state is found not only in thylakoids but also in PSII-enriched membrane fragments as well as in purified core complexes, from both spinach and cyanobacteria (unpublished results). The relative contribution of the slow phase with respect to the fast phase in all cases follows closely the expected ratio of 0.43:0.57 ($^{34}k_1$:$^{34}k_2$) based on the isotopic equilibrium distribution between two separate exchanging sites (*20*). This observation clearly indicates that the two sites retain their relative rates of exchange in all of the S states and that there is not a conversion of a slow exchange site into a fast exchange site, or vice versa, during the S-state cycle. For if there was a conversion, the two sites would become isotopically equilibrated with each other during the *turnover* flash sequence times and would result in marked variations in the relative contributions of the two kinetic phases.

Most importantly, the slow phase kinetics in the $m/e = 34$ data are confirmed by the corresponding measurements of the ^{18}O isotopic exchange at $m/e = 36$ which reveal only a single kinetic phase and a rate constant virtually identical as determined for the slow phase (Table 1) [The scatter in the S_0 data is sufficiently large to exclude identical rate constants between the $m/e = 36$ and $m/e = 34$ data, but the difference is less than a factor of 2. Cross-correlation of the two data sets yields a rate constant of $14 \pm 2\ s^{-1}$.] This result shows conclusively that the overall incorporation of ^{18}O into the O_2 that is produced is limited throughout the S-state cycle by the substrate water undergoing the slow isotopic exchange process and that the biphasic behavior in the $m/e = 34$ measurements *does not* arise from PSII heterogeneity. Thus, from Table 1, it is clear that the rate of slow exchange ($^{34}k_1$) first slows down by a factor of ~500 on the S_0 to S_1 transition, then speeds up by a factor of ~100 on the S_1 to S_2 transition, and remains unchanged on the S_2 to S_3 transition.

In contrast, the second, fast phase of exchange in the $m/e = 34$ data becomes resolvable under our present experimental setup only in the S_3 state while its kinetics in the S_2, S_1, and S_0 states are equal to or faster than the injection response (i.e., $k_{inj} = 175\ s^{-1}$) or the total *turnover* sequence time (i.e., $k_t = 100\ s^{-1}$). Based on the time resolution of our measurements, the rate of fast exchange ($^{34}k_2$) slows down by at least a factor of 5 during the S_2 to S_3 transition, while as described above, the rate of slow exchange ($^{34}k_1$) does not undergo any observable alteration during the same transition. It is thus apparent from these results that the biphasic ^{18}O isotopic exchange kinetics reflect separate substrate binding sites whose affinities vary independently through the S-state cycle.

DISCUSSION

Critical questions concerning the understanding of the photosynthetic O_2 evolving mechanism include at which step(s) and in what form do the two substrate water molecules bind during the S-state cycle and how is the O−O bond generated. Our results on the complete S-state dependence of the ^{18}O exchange in PSII (Figure 2, Table 1) have an important bearing on these questions and can be summarized as follows: (1) the rate for the slow isotopic exchange process ($^{34}k_1$) decreases during the S_0 to S_1 transition and increases during the S_1 to S_2 transition but stays the same during the S_2 to S_3 transition, while the rate of the fast isotopic exchange process ($^{34}k_2$) decreases by a factor of 5 or more on at least the S_2 to S_3 transition; (2) in the S_3 state, the two isotopic exchange processes exhibit rates slower than the O_2 release time of 1−2 ms (*24, 25*); and (3) throughout the S-state cycle, the isotopic exchange processes are all remarkably fast, with the slowest exchange process being measured in the S_1 state with a $t_{1/2} \sim 50$ s.

The observations that the rates of ^{18}O exchange vary with the S states and are all relatively fast strongly support the notion that the substrate water is bound to the functional

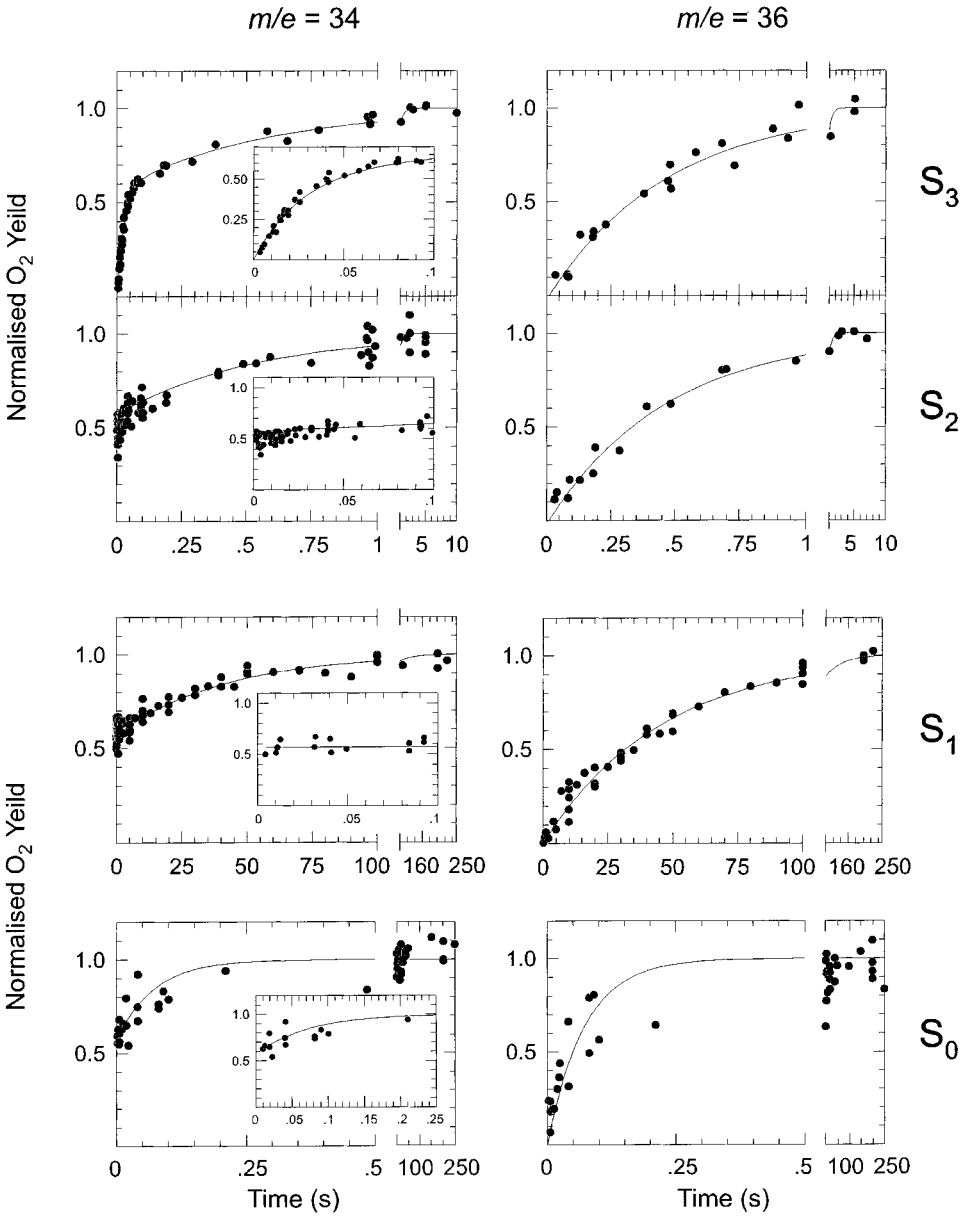

FIGURE 2: Complete S-state dependence for the ^{18}O isotopic exchange between added $H_2{}^{18}O$ and the O_2 produced by photosystem II in spinach thylakoid samples. Mass measurements were made at $m/e = 34$ for the mixed labeled $^{16}O^{18}O$ product (left panels) and at $m/e = 36$ for the double labeled $^{18}O^{18}O$ product (right panels) at 10 °C. Each curve represents the summation of 4−7 data sets. In many of the measurements, the $m/e = 34$ and $m/e = 36$ data were collected simultaneously. The solid lines represent best fits to the data points based on eqs 3 and 4 for the $m/e = 36$ and $m/e = 34$ data, respectively, as described in the text. Note the different time axes between the upper and lower panels. Data for the S_3 and S_2 states have been reported earlier (*19*, *20*). See text for details.

Table 1: Rate Constants for ^{18}O Exchange in Spinach Thylakoid Samples as a Function of the S States at 10 °C[a]

S state	^{36}k (s^{-1})	$^{34}k_1$ (s^{-1})	$^{34}k_2$ (s^{-1})
S_3	2.1 ± 0.2	1.9 ± 0.2	36.8 ± 1.9
S_2	2.2 ± 0.1	1.9 ± 0.3	>175
S_1	0.022 ± 0.002	0.021 ± 0.002	>100
S_0	18 ± 3	8 ± 2	>100

[a] See text for details.

Mn ions as labile terminal ligands rather than as tightly bound bridging ligands. In general, for metal−water complexes, the rate of isotopic exchange slows down, and the binding affinity increases, as the metal center becomes oxidized and the ionic radius of the complex decreases (*26*). Thus, the decrease in $^{34}k_1$ from ∼8 to ∼0.021 s^{-1} during the S_0 to S_1 transition (Table 1) would be consistent with a formal oxidation increase at a Mn binding site. Indeed, recent XANES and EPR measurements do suggest that a Mn^{II} ion is oxidized to a Mn^{III} ion during this transition (*27*−*30*). However, based on the magnitude of $^{34}k_1$ in the S_0 state (∼10^1 s^{-1}, see Table 1), we feel that the substrate water molecule is unlikely to be bound to a Mn^{II} ion since the rate of exchange in Mn^{II}−water complexes is in general expected to be much faster (∼10^7 s^{-1}) (*31*). Rather, in comparison with other hydrated metal complexes (*20*, *32*), we believe the magnitude of $^{34}k_1$ in the S_0 state is best interpreted as water bound to a Mn^{III} ion. If this is the case, then the decrease in $^{34}k_1$ during the S_0 to S_1 transition would have to be due to another mechanism, such as a p*K* shift in the complex. Based on Mn model compounds, an increase in oxidation can lower the p*K* by as much as 8 pH units (*33*). Thus, if a neighboring Mn^{II} ion in the OEC is oxidized to

Mn^{III}, the resulting decrease in p*K* could lead to a deprotonation of the bound substrate water and thereby cause a decrease in the ^{18}O exchange rate.

In contrast to the S_0 to S_1 transition, the S_1 to S_2 transition is commonly held to be coupled to the oxidation of a Mn^{III} ion to a Mn^{IV} ion, to explain the characteristic S_2-state Mn EPR signals (*2*). But, surprisingly, the $^{34}k_1$ *increases* by a factor of ~100, from ~0.02 to ~2.0 s^{-1} (Table 1), during this transition. Clearly, this finding shows that the site which binds the slowly exchanging substrate water ligand *is not* the Mn ion which undergoes the oxidation increase to produce the S_2-state Mn EPR signals. To account for the unexpected increase in the $^{34}k_1$ during the S_1 to S_2 transition, we note that individual metal ions (*31*) and μ-hydroxo-bridged complexes (*34*) can show significant enhancements in water exchange rate upon deprotonation of adjacent ligands. Thus, an attractive hypothesis would be the deprotonation of a μ-hydroxo bridge in the Mn cluster during the S_1 to S_2 transition. Unfortunately, current EXAFS measurements do not show a corresponding change in the Mn−Mn distance during this transition that would be indicative of such a deprotonation event (*6*). Alternatively, the deprotonation may occur at a different bridging site in the OEC. For example, recent FTIR evidence suggests that the ligation of the Mn cluster undergoes a significant reorganization upon the selective breakage of a carboxylate bridge during the S_1 to S_2 transition (*35*).

Interestingly, the magnitude of $^{34}k_1$ in the S_2 state is identical to the magnitude of $^{34}k_1$ in the S_3 state (Table 1). This observation shows that the affinity of the binding site for this substrate water molecule stays the same during the S_2 to S_3 transition despite the further accumulation of an oxidizing equivalent in the OEC. However, the exchange at the second substrate binding site, which is unresolvable in the S_2 and earlier S states by our current experimental setup, slows down by at least a factor of 5, to yield a rate constant of $^{34}k_2 \sim 37$ s^{-1} in the S_3 state (Table 1). The decrease in $^{34}k_2$ during this step would again be consistent with a metal-centered oxidation increase or a deprotonation of the bound water. Unfortunately, it is still controversial as to whether a Mn-centered oxidation takes place on the S_2 to S_3 transition. Based on XANES measurements, one research group has argued that a formal Mn oxidation increase does indeed occur (*30*) while another group has argued in favor of a ligand-centered oxidation (*27*; J. Messinger, personal communication). In either case, it is important to note that only $^{34}k_2$ is affected during the S_2 to S_3 transition, and not $^{34}k_1$. This observation provides strong evidence that the two binding sites are chemically separate in the S_3 state.

Our overall results can be illustrated by the scheme shown in Figure 3. Here, the Mn ions of the OEC are shown to be organized into two types: (1) those which are involved in the direct accumulation of oxidizing equivalents (designated by the brackets) and (2) those which are involved in substrate binding. In the scheme, a Mn ion is proposed to bind a substrate water molecule beginning in the S_0 state and accounts for the slow ^{18}O exchange kinetics that are observed throughout the S states. This Mn site is assumed not to undergo any formal metal-centered oxidations up to the S_3 state, though, as indicated, it could undergo a transient oxidation increase in the S_4 state. Based on the magnitudes of the exchange rates measured, this site is likely to be a

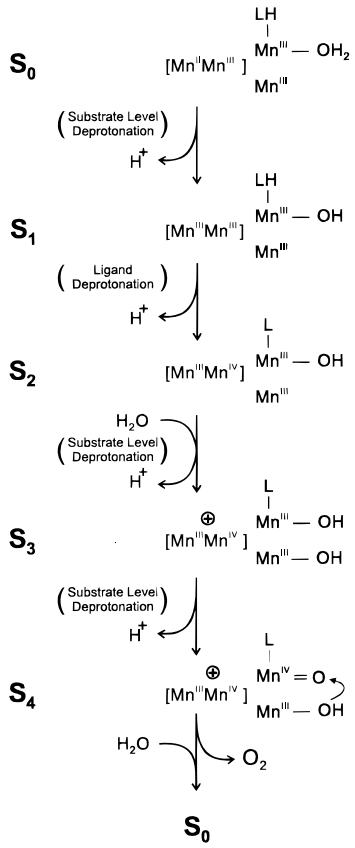

FIGURE 3: A proposed scheme for the O_2 evolving complex in photosystem II to explain the S-state dependence in the ^{18}O exchange kinetics. The four Mn ions are organized such that only two are associated with the accumulation of oxidation equivalents during the S-state turnover while the other two Mn ions are involved with the binding of the substrate water. The changes in the isotopic exchange and binding affinities are ascribed to deprotonation events, either at the substrate water itself or at adjacent ligands, which result from a successive decreases in the p*K* of the Mn_4 cluster as a whole upon S-state turnover. Proton rearrangements are only implied at the catalytic site and do not necessarily reflect direct proton release into the bulk. The second substrate water molecule is proposed to only enter into the reaction sequence during the S_2 to S_3 transition when the binding site becomes 'open' to the solvent water. See text for further discussion.

Mn^{III} ion, having either a nonoctahedral symmetry or a non-Jahn−Teller lengthened bond with the water ligand, and not a Mn^{IV} ion. In the latter case, the unprotonated terminal oxo ligands that are normally favored by the strong basicity of the Mn^{IV} ion (*36*) are inconsistent with the relatively fast rates of isotopic exchange that we observe.

In the scheme of Figure 3, the fast exchanging substrate site is also predicted to be a Mn^{III} ion, mainly because the magnitude of its ^{18}O exchange in the S_3 state is not dramatically different from that for the slow exchanging site. However, since we cannot currently resolve $^{34}k_2$ in the S_0, S_1, and S_2 states, it is possible that water only enters this binding site during the S_2 to S_3 transition. In this situation, substrate accessibility to the Mn_4 cluster as regulated by the surrounding protein structure would be important. Indeed, Mn EXAFS measurements have been interpreted to indicate the occurrence of a structural change during the S_2 to S_3 transition (H. Dau, unpublished data). The role of substrate accessibility may be to optimize the redox poise and the positioning of the reactants in the reaction mechanism such that O_2 is favored over the formation of other possible

intermediates such as hydrogen peroxide (*37*). Alternatively, the water molecule at the fast exchanging site may also be bound in the S_0 state but undergoes very fast isotopic exchange until the S_3 state. This could occur if the fast exchanging site is a Mn^{III} ion with a Jahn−Teller lengthened bond to the substrate water or is a Ca^{II} ion. In either case, O−O bond formation must still take place during the final S_3 to S_4 to S_0 transition where it may occur as a nucleophilic attack by the substrate water at the fast exchanging site on the substrate water at the slow exchanging site through a concerted electron transfer, as suggested earlier (*19*).

The suggestion that Mn^{III} ions in the OEC constitute the substrate binding sites throughout the S-state cycle need not necessarily be at odds with the XANES data on the Mn oxidation states. It has been argued that the Mn edge positions strongly depend on the O/N ratio of the surrounding ligands (R. Pace, personal communication) and on the coordination geometry (*38*) as well as on the formal oxidation state (*39*); thus, the Mn oxidation states interpreted from the XANES data are not necessarily unique, at least until an exact structure of the complex is known. Therefore, to avoid the generation of extreme Mn oxidation levels in the higher S states in the scheme of Figure 3, we propose that in the S_1 state all four Mn ions exist in the +3 oxidation state. During the S_1 to S_2 transition, there would be an oxidation of a Mn^{III} to a Mn^{IV} to account for the S_2-state EPR signals while during the S_2 to S_3 transition the accumulation of the oxidizing equivalent could occur either as a metal-centered or as a ligand-centered oxidation. These latter possibilities are merely indicated in Figure 3 by the + symbol above the Mn pair which accumulates the oxidation equivalents.

By assigning different sets of Mn ions with low oxidation states to the accumulation of oxidizing equivalents and to substrate binding, we can accommodate both the XANES and ^{18}O exchange data. The variations in the ^{18}O exchange rates with the S states can then be explained in terms of the protonation status of the complex, either of the substrate water itself or of adjacent ligands, as discussed above. The separation of the accumulation of oxidation equivalents from substrate binding and O−O bond formation is an extension of an earlier hypothesis in which a special 'water-binding component' in the OEC was invoked to account for the observed disconnection of O_2 evolution from S-state turnover in the presence of certain lipophilic compounds (*40*). However, regardless of the details, our results are largely inconsistent with most current models of O_2 evolution, either because the observed changes in the ^{18}O exchange during the early S-state transitions are incompatible with the expected binding affinities in these models (*7*, *11*) or because the models do not account for the independent kinetic behavior of the two binding sites upon the S_2 to S_3 transition (*8*−*10*, *12*, *41*, *42*).

CONCLUSIONS

The results from the complete S-state dependence of the ^{18}O exchange measurements of photosystem II lead to the following conclusions: (1) at least one substrate water molecule is bound to the O_2 evolving complex throughout the entire S-state cycle at a site which is chemically distinct from the site that binds the second substrate water molecule; (2) if Mn ions form the binding sites for the substrate water, then at least two of the Mn ions must function *independently* of each other within the catalytic cluster; (3) the O−O bond forming step must occur during the final S_3 to S_4 to S_0 transition; and (4) although the variations in the substrate binding affinities during the S-state cycle are not straightforward, they probably reflect deprotonation reactions and dynamic structural changes at the catalytic site rather than direct metal-centered oxidations at the substrate binding sites. We feel that our findings provide some surprising insights into the photosynthetic O_2 evolution and will need to be addressed in future chemical mechanisms.

ACKNOWLEDGMENT

We gratefully thank Alan Sargeson, Stephen Lincoln, Ron Pace, and Johannes Messinger for many fruitful discussions and advice in this work and Murray Badger for technical assistance in the use of the mass spectrometer.

REFERENCES

1. Rhee, K.-H., Morris, E. P., Barber, J., and Kühlbrandt, W. (1998) *Nature 396*, 283−286.
2. Britt, D. R. (1996) in *Oxygenic Photosynthesis: The Light Reactions* (Ort, D. R., and Yocum, C. F., Eds.) pp 137−164, Kluwer Academic Publishers, Dordrecht, The Netherlands.
3. Diner, B., and Babcock, G. T. (1996) in *Oxygenic Photosynthesis: The Light Reactions* (Ort, D. R., and Yocum, C. F., Eds.) pp 213−247, Kluwer Academic Publishers, Dordrecht, The Netherlands.
4. Joliot, P., Barbieri, G., and Chaubaud, R. (1969) *Photochem. Photobiol. 10*, 309−329.
5. Kok, B., Forbush, B., and McGloin, M. (1970) *Photochem. Photobiol. 11*, 457−475.
6. Yachandra, V. K., Sauer, K., and Klein, M. P. (1996) *Chem. Rev. 96*, 2927−2950.
7. Hoganson, C. W., and Babcock, G. T. (1997) *Science 277*, 1953−1956.
8. Pecoraro, V. L., Baldwin, M. J., Caudle, M. T., Hsieh, W.-Y., and Law, N. A. (1998) *Pure Appl. Chem. 70*, 925−929.
9. Smith, P. J., Åhrling, K. A., Razeghifard, M. R., and Pace, R. J. (1998) in *Photosynthesis: Mechanisms and Effects* (Garab, G., Ed.) pp 1363−1366, Kluwer Academic Publishers, Dordrecht, The Netherlands.
10. Limburg, J., Szalai, V. A., and Brudvig, G. W. (1999) *J. Chem. Soc., Dalton Trans. 1999*, 1353−1361.
11. Haumann, M., and Junge, W. (1999) *Biochim. Biophys. Acta 1411*, 86−91.
12. Siegbahn, P. E. M., and Crabtree, R. H. (1999) *J. Am. Chem. Soc. 121*, 117−127.
13. Tommos, C., and Babcock, G. T. (1998) *Acc. Chem. Res. 31*, 18−25.
14. Ahlbrink, R., Haumann, M., Cherepanov, D., Bögerhausen, O., Mukidjanian, A., and Junge, W. (1998) *Biochemistry 37*, 1131−1142.
15. Hillier, W., Lukins, P., Seibert, M., and Wydrzynski, T. (1997) *Biochemistry 36*, 76−85.
16. Radmer, R., and Ollinger, O. (1980) *FEBS Lett. 110*, 57−61.
17. Radmer, R., and Ollinger, O. (1986) *FEBS Lett. 195*, 285−289.
18. Bader, K. P., Thibault, P., and Schmid, G. H. (1987) *Biochim. Biophys. Acta 893*, 564−571.
19. Messinger, J., Badger, M., and Wydrzynski, T. (1995) *Proc. Natl. Acad. Sci. U.S.A. 92*, 3209−3213.
20. Hillier, W., Messinger, J., and Wydrzynski, T. (1998) *Biochemistry 37*, 16908−16914.
21. Hillier, W., Messinger, J., and Wydrzynski, T. (1998) in *Photosynthesis: Mechanisms and Effects* (Garab G., Ed.) pp 1307−1310, Kluwer Academic Publishers, Dordrecht, The Netherlands.
22. Messinger, J., Schröder, W., and Renger, G. (1993) *Biochemistry 32*, 7658−7668.

23. Hillier, W. (1999) Ph.D. Thesis, The Australian National University, Canberra, Australia.
24. Lavorel, J. (1992) *Biochim. Biophys. Acta 1101*, 33−40.
25. Razeghifard, M. R., and Pace, R. J. (1999) *Biochemistry 38*, 1252−1257.
26. Lincoln, S. F., and Merbach, A. E. (1995) *Adv. Inorg. Chem. 42*, 1−88.
27. Roelofs, T. A., Liang, W., Latimer, M. J., Cinco, R. M., Rompel, A., Andrews, J. C., Sauer, K., Yachandra, V. K., and Klein, M. P. (1996) *Proc. Natl. Acad. Sci. U.S.A. 93*, 5230−5238.
28. Åhrling, K. A., Peterson, S., and Styring, S. (1997) *Biochemistry 36*, 13148−13152.
29. Messinger, J., Nugent, J. H. A., and Evans, M. C. W. (1997) *Biochemistry 36*, 11055−11061.
30. Luzzolino, L., Dittmer, J., Dörner, W., Meyer-Klaucke, W., and Dau, H. (1998) *Biochemistry 37*, 17112−17119.
31. Ducommun, Y., Newman, K. E., and Merbach, A. E. (1980) *Inorg. Chem. 19*, 3696−3703.
32. Pecoraro, V. L. (1988) *Photochem. Photobiol. 48*, 249−264.
33. Caudle, M. T., and Pecoraro, V. L. (1997) *J. Am. Chem. Soc. 119*, 3415−3416.
34. Crimp, S. L., Spiccia, L., Krouse, H. R., and Swaddle, T. W. (1994) *Inorg. Chem. 33*, 465−470.
35. Noguchi, T., Ono, T.-A., and Inoue, Y. (1995) *Biochim. Biophys. Acta 1228*, 189−200.
36. Comba, P., and Merbach, A. (1987) *Inorg. Chem. 26*, 1315−1323.
37. Wydrzynski, T., Hillier, W., and Messinger, J. (1996) *Physiol. Plant. 96*, 342−350.
38. Zheng, M., and Dismukes, G. C. (1996) *Inorg. Chem. 35*, 3307−3319.
39. Sauer, K., Yachandra, V. K., Britt, R. D., and Klein, M. P. (1992) in *Manganese Redox Enzymes* (Pecoraro, V. L., Ed.) pp 141−175, VCH Publishers, New York.
40. Wydrzynski, T., Huggins, B. J., and Jursinic, P. A. (1985) *Biochim. Biophys. Acta 809*, 125−136.
41. Karge, M., Irrgang, K.-D., and Renger, G. (1997) *Biochemistry 36*, 8904−8913.
42. Schlodder, E. and Witt, H. T. (1999) *J. Biol. Chem. 274*, 30387−30392.

BI992318D